



**TITLE**

**The immunophilin Zonda controls regulated exocytosis in endocrine and exocrine tissues.**

**RUNNING TITLE**

**Zonda regulates exocytosis**

**AUTHORS:**

**Rocío de la Riva Carrasco<sup>\*, a</sup>, Sebastián Perez Pandolfo<sup>\*, a</sup>, Sofía Suarez Freire<sup>a</sup>, Nuria M. Romero<sup>c, d, e</sup>, Zambarlal Bhujabal<sup>f</sup>, Terje Johansen<sup>f</sup>, Pablo Wappner<sup>#, a, b, g</sup>, Mariana Melani<sup>#, a, b</sup>**

**CONTACT INFORMATION:**

**<sup>a</sup> Fundación Instituto Leloir, Buenos Aires 1405, Argentina.**

This article has been accepted for publication and undergone full peer review but has not been through the copyediting, typesetting, pagination and proofreading process which may lead to differences between this version and the [Version of Record](#). Please cite this article as doi: [10.1111/tra.12777](https://doi.org/10.1111/tra.12777)

<sup>b</sup> Consejo Nacional de Investigaciones Científicas y Tecnológicas (CONICET), Buenos Aires, Argentina.

<sup>c</sup> Université Côte d'Azur, INRA, CNRS, Institut Sophia Agrobiotech, 06900 Sophia Antipolis, France.

<sup>d</sup> CNRS, Institute of Biology Valrose, Parc Valrose, 06108 Nice, France.

<sup>e</sup> INSERM, Institute of Biology Valrose, Parc Valrose, 06108 Nice, France.

<sup>f</sup> Molecular Cancer Research Group, Department of Medical Biology, University of Tromsø—The Arctic University of Norway, 9037 Tromsø, Norway.

<sup>g</sup> Departamento de Fisiología, Biología Molecular y Celular, Facultad de Ciencias Exactas y Naturales—Universidad de Buenos Aires, 1428 Buenos Aires, Argentina.

\* Should be considered joint first author

# Corresponding authors

[pwappner@leloir.org.ar](mailto:pwappner@leloir.org.ar)

[mmelani@leloir.org.ar](mailto:mmelani@leloir.org.ar)

## SYNOPSIS

The immunophilin Zonda acts at the final stages of exocytosis by regulating fusion of the exocytic granule to the plasma membrane.

## ABSTRACT

Exocytosis is a fundamental process in physiology, communication between cells, organs and even organisms. Hormones, neuropeptides and antibodies, among other cargoes are packed in exocytic vesicles that need to reach and fuse with the plasma membrane to release their content to the extracellular milieu. Hundreds of proteins participate in this process and several others in its regulation. We report here a novel component of the exocytic machinery, the *Drosophila*

transmembrane immunophilin Zonda (Zda), previously found to participate in autophagy. Zda is highly expressed in secretory tissues, and regulates exocytosis in at least three of them: the ring gland, insulin-producing cells and the salivary gland. Using the salivary gland as a model system, we found that Zda is required at final steps of the exocytic process for fusion of secretory granules to the plasma membrane. In a genetic screen we identified the small GTPase RalA as a crucial regulator of secretory granule exocytosis that is required, similarly to Zda, for fusion between the secretory granule and the plasma membrane.

#### **KEY WORDS**

Exocytosis; *Drosophila*, Zonda, Immunophilin, RalA, Salivary Gland, Secretory Granule

#### **ACKNOWLEDGMENTS**

We are grateful to Dr. Andrew Andres, Dr. Gabor Juhasz, the Bloomington Stock Centre and the Vienna *Drosophila* Resource Centre for fly strains. Dr. Pierre Leopold for sharing the anti-Dilp2 antibody, Dr. Andrés Rossi for technical support with confocal microscopy, Andrés Licerí for fly food preparation, the FIL personnel for assistance, and members of the Wappner lab for discussions.

## INTRODUCTION

Exocytosis is a fundamental cellular process required for delivery of proteins, lipids and carbohydrates to the extracellular milieu, so hormones, antibodies and neuropeptides, among others, are released from the cells where they are produced by this mechanism. The exocytic process requires the genesis of secretory vesicles in which export products are packed. These vesicles sprout from the trans-Golgi network in an immature exocytosis-incompetent state, and thereafter, vesicles undergo maturation, in a process that includes homotypic fusion, condensation and acidification of their content. During this process, incorporation of specific vesicle membrane proteins occurs, including SNARES and Synaptotagmins required for membrane fusion. Then, mature exocytic vesicles or secretory granules (SGs) are directionally transported to the cellular apical domain, where prior to secretion, a series of events that include tethering, priming, triggering and fusion to the plasma membrane take place, each of them executed by specific molecular complexes and their regulators <sup>1</sup>.

Most cellular models for studying exocytosis rely on the analysis of a sole readout: Intracellular accumulation of SGs and/or exocytosis of SG content. The salivary gland of *Drosophila melanogaster* larvae is a useful model to study the mechanisms involved in exocytosis <sup>2,3</sup>. At late 3<sup>rd</sup> larval instar, salivary glands synthesize a series of mucins called Glue proteins that are packed into SGs, known as Glue granules (GGs). Immature GGs initially sprout from the trans-Golgi network (TGN) as 1 $\mu$ m diameter vesicles, reaching then a mature size of around 5 $\mu$ m after several events of homotypic fusion and maturation <sup>4,5</sup>. At the onset of pupariation GGs undergo exocytosis and Glue proteins are released to the salivary gland lumen, from where they are later secreted to adhere the puparium to the substratum <sup>2,6</sup>. Recently, the final steps of GG exocytosis at the salivary gland were described in detail. Fusion of the GG to the Apical Plasma Membrane (APM) results in transfer of the lipid phosphatidylinositol 4,5-bisphosphate (PI(4,5)P<sub>2</sub>) from the APM to the GG membrane, an

event that enables recruitment of the small GTPase Rho1 to the GG, followed by simultaneous activation of Diaphanous (Dia) and Rho-associated kinase (Rok) on the GG membrane. These events result in polymerization of an acto-myosin mesh around the GGs, which is critical for efficient release of GG content into the salivary gland lumen <sup>7,8</sup>. However, our knowledge on how GGs fuse with the plasma membrane remains incomplete.

FK506-binding proteins (FKBPs) are immunophilins that can bind the immunosuppressant KF506, and display peptidyl-prolyl *cis/trans* isomerase activity (PPIase). FKBPs participate in a myriad of cellular activities, including protein folding, receptor signaling and transcription <sup>9,10</sup>. FKBP8 is a non-canonical member of this family, as its PPIase activity depends on binding to Ca<sup>++</sup>-conjugated Calmodulin, and includes a transmembrane domain on its carboxy-terminus, a unique feature among FKBPs <sup>9,11</sup>. FKBP8 has been reported to interact with several proteins such as Bcl-2, Bcl-XL <sup>12,13</sup>, HSP90 <sup>14,15</sup>, Rheb <sup>16</sup>, PDH2 <sup>17</sup> and LC3 <sup>11</sup>. In this way, FKBP8 regulates diverse cellular processes, including apoptosis, mitophagy and hypoxic responses. Previously, we have characterized the function of Zonda (Zda), the predicted *Drosophila* FKBP8 ortholog, as a key regulator of early steps of autophagy <sup>18</sup>.

In this work we report a novel function for the transmembrane immunophilin Zda in regulated exocytosis in different secretory tissues, including the prothoracic gland (PG), insulin producing cells (IPCs) of the brain, and salivary glands. Detailed analysis of Zda loss-of-function phenotypes at the salivary gland revealed that it is required for GG fusion with the plasma membrane, but not for their biogenesis or maturation. Through a genetic screen of components known to participate in secretory granule fusion to the plasma membrane, we identified the small GTPase Ra1A as a key player in GG exocytosis, which genetically interacts with Zda.

## RESULTS

## Zonda is expressed in secretory tissues

We made use of the allele *zda<sup>trojan</sup>* to gain insights into the tissues in which *zda* is expressed. *zda<sup>trojan</sup>* insertion generates a truncated product (Supplementary Figure 1A), and therefore renders a null allele that is lethal in homozygosis, which does not complement with another previously characterized *zda* null allele (*zda<sup>null</sup>*)<sup>18</sup>. Moreover, expression of a UAS-*mCh-zda* construct driven by *zda<sup>trojan</sup>* completely restored viability, strengthening the notion that *zda<sup>Trojan</sup>* is a genuine loss-of-function allele, and that mCh-Zda is fully functional. Interestingly, overexpression of truncated versions of mCh-Zda, lacking its transmembrane domain (mCh-Zda<sup>ΔTM</sup>) or its calmodulin/TPR domain (mCh-Zda<sup>ΔCaM/ΔTPR</sup>), failed to rescue lethality of the *zda<sup>Trojan</sup>* allele, indicating that these domains are required for Zda function (Supplementary Figure 1B, C).

*zda<sup>trojan</sup>* contains a gene trap cassette, derived from a MiMIC insertion in *zda*'s second intron (Supplementary Figure 1A). The cassette includes a Trojan GAL4 exon composed of a splice acceptor, a T2A peptide, a GAL4 coding sequence and an Hsp70 transcription termination signal<sup>19</sup>. We crossed this allele with a UAS-mCD8-GFP reporter, and observed that *zda* is highly expressed in glandular tissues and secretory cells, among other organs, as previously reported by high-throughput anatomy RNA-seq data<sup>20</sup>. We detected strong expression in the salivary glands, the ring gland (RG), the lymph gland, insulin producing cells (IPC) of the brain, a subset of cells of the intestine, and secondary cells of the adult male accessory gland (Figure 1A-F). The fat body also displayed high expression levels, as also did differentiated cells of the eye imaginal disc, posterior to the morphogenetic furrow (Figure 1 G, H). Other imaginal discs, such as the wing disc showed no significant expression of *zda<sup>Trojan</sup>* under the same imaging conditions (Figure 1I). The ejaculatory duct also displayed high expression levels (Figure 1J), unlike the testis where expression was minimal (Figure 1K), while no significant expression was observed in adult ovaries (Figure 1L). Since *zda* is expressed at high levels

in several tissues or cell types with secretory function, we sought to explore a possible role of Zda in exocytosis.

### **Zonda is required for exocytosis of ecdysone, Insulin-like peptide 2 and Glue proteins**

We hypothesized that the *zda* expression pattern might reflect a function of Zda in secretion. We therefore analyzed Zda function in the RG, IPCs and salivary glands. The RG is composed of three different cell types specialized in secretion of specific products. The prothoracic gland (PG) encompasses most of the RG, and is dedicated to biosynthesis and secretion of the steroid hormone 20-hydroxy ecdysone (20E)<sup>21</sup>. Also, PG cells can be readily distinguished from other RG cell types as they are innervated by axons of PTTH-producing neurons. As depicted in Figure 2A, *zda* is highly expressed in PG cells that are innervated by PTTH axons. To test if Zda might be involved in 20E exocytosis, we expressed a *zda* RNAi using the PG driver *phantom*-Gal4, and observed a significant delay in pupariation time as compared to controls (Figure 2B). Supplementation of the culture medium with 20E resulted in complete rescue of normal pupariation time (Figure 2B), suggesting that Zda knock down in PG cells results in reduced levels of circulating 20E<sup>21</sup>.

To investigate if the above Zda loss-of-function phenotype may arise from impaired 20E secretion, we determined the levels of circulating 20E relative to the total 20E larval content, and found that Zda silencing in the PG results in 3.5 times reduction of circulating 20E (Figure 2C). It was recently shown that after being synthesized in PG cells, ecdysone is packaged in secretory vesicles, and released to the extracellular milieu by exocytosis<sup>21</sup>. As these vesicles are Synaptogamin-1 (Syt-1) positive, we analyzed the presence of Syt-1-GFP vesicles in PG cells of control *versus* *zda* RNAi-expressing wandering larvae. In control individuals, we observed few intracellular Syt1-GFP positive vesicles as previously reported<sup>21</sup>, with most of the Syt-1-GFP label localized at the plasma membrane (Figure 2D, F), suggesting that most vesicles have successfully fused with the plasma membrane, and released their content. In contrast, in Zda-deficient PG cells, Syt-1-GFP-positive vesicles could be readily detected intracellularly, while almost no Syt-1-GFP was observed at the

plasma membrane (Figure 2E, F), suggesting that exocytosis is impaired in these PGs. We thus conclude that *Zda* is required at the PG for exocytosis of Syt-1-positive ecdysone-containing vesicles.

To further evaluate a possible role of *Zda* in regulated exocytosis, we turned to the IPCs. IPCs are brain neurosecretory cells clustered in two groups of 7 cells each that produce and secrete insulin-like peptides (dILPs), which are released to the hemolymph in response to hormonal or environmental stimuli, and regulate body growth<sup>22</sup>. We first confirmed that *zda* is highly expressed in IPCs, as its expression colocalizes with that of *Dilp2*<sup>23</sup>(Figure 3A). Next, we tested if *Zda* is required for dILP secretion by knocking down its expression in IPCs with a *dilp2*-Gal4 driver. This silencing resulted in significant reduction of pupal volume (Figure 3B), which is characteristic of diminished levels of circulating dILPs. Consistent with this, dILP2 levels were significantly higher inside the IPCs in well-fed *zda*<sup>RNAi</sup> larvae, as compared to wild type controls in which dILP2 was detected at high levels in IPCs of starved, but not of well-fed larvae (Figure 3C, D). These results suggest that *Zda* is required at the IPCs for dILP2 exocytosis.

Finally, we looked at exocytosis of Glue granules (GGs) in larval salivary glands. GGs are exocytic vesicles packed with mucins named Salivary Gland Secretion (SGS) that serve to adhere the animal to the substratum at the time of pupariation<sup>2</sup>. GGs form in response to an ecdysone peak at the onset of the larval wandering stage, and are exocytosed in response to a later ecdysone peak at the time of puparium formation<sup>2</sup>. To evaluate exocytosis of GGs, we utilized a transgenic line that expresses one of the SGSs, SGS3, fused to GFP (SGS3-GFP)<sup>2</sup>. In wandering larvae, salivary glands normally contain large amounts of SGS3-GFP (Figure 4A, A'), while after pupariation, SGS3-GFP is exocytosed to the lumen of the gland and released outside of the puparium (Figure 4B, B', E). When *Zda* was downregulated in salivary glands, we found normal levels of SGS3-GFP in salivary glands of wandering larvae, indicating that the mucin is normally produced (figure 4C, C'), while at the



prepupal stage SGS3-GFP failed to be secreted, and remained inside the gland (Figure 4D, D', E). These observations suggest that Zda is required at the salivary gland for exocytosis of GGs. To analyze if this is the case, we dissected salivary glands of control and Zda knock down prepupae, and observed that, whereas control salivary glands do not contain GGs (Figure 4F), in Zda knock down salivary gland cells, a large number of GGs were present (Figure 4G). These results indicate that Zda is required for GG exocytosis in salivary glands, and more generally, that Zda regulates exocytosis in exocrine and endocrine glands.

#### **Zonda is required for GG fusion with the plasma membrane**

We utilized the salivary gland to study in more detail the role that Zda plays in exocytosis. GGs emanate from the Trans Golgi Network as 1  $\mu\text{m}$  vesicles, and reach a mature size of 5  $\mu\text{m}$  prior to fusion with the APM<sup>5</sup>. We compared GG diameter in salivary glands of Zda knock down and control wandering larvae, just prior to the stage when exocytosis is expected, and observed that GG size was not altered (Figure 5A-C), suggesting that Zda is not required for GG biogenesis or maturation.

PI(4,5)P<sub>2</sub> is a lipid of the inner leaflet of the plasma membrane, absent from intracellular organelles<sup>24</sup>. Upon fusion of mature GGs with the APM, PI(4,5)P<sub>2</sub> incorporates to the membrane of the GG, and this lipid transfer can be followed by looking at the PI(4,5)P<sub>2</sub> reporter PLC $\delta$ PH-EGFP<sup>7,8</sup>. GG fusion to the APM triggers the formation of a filamentous actin mesh around the GG that can be readily detected by life-act-Ruby or phalloidin<sup>7,8</sup>, so that only mature GGs that successfully fuse with the APM are positive for PI(4,5)P<sub>2</sub> and actin markers (Figure 5D-F, G). Both PI(4,5)P<sub>2</sub> and actin recruitment to GGs were significantly reduced in Zda knock down larvae (Figure 5E-G), suggesting that Zda is required for fusion of GGs to the APM.

To confirm that in Zda-KD salivary glands, GGs fail to fuse with the plasma membrane, we acquired high magnification Z-stacks images of mature GGs in close proximity to the APM. In control salivary glands, a fusion neck connecting the APM with the GG could be clearly observed, being

these granules in most cases surrounded by an actin mesh (Figure 5H, Supplementary Figure 4 and Supplementary Video 1). In contrast, in Zda-deficient glands, the GGs were not surrounded by the actin mesh, and although they could be observed in close proximity of the APM, they were not physically connected with it (Figure 5I, Supplementary Figure 4 and Supplementary Video 2). Three-dimension reconstruction of Z-stacks clearly allowed us to see no contact sites between GG and APM in Zda-KD salivary glands. Fusion with the APM modifies the GG content appearance<sup>7</sup>: Prior to fusion with the APM, the content of GGs appears bright and heterogeneous, while after fusion, fluorescence loses intensity and becomes homogenous (Supplementary Figure 5A-B). We utilized this criterion to score the number of GGs that have fused with the APM, and found that this number was reduced to less than one third in Zda KD larvae in comparison to wild type controls (Supplementary Figure 5B-D). Altogether, our data show that, in the exocytic process, Zda is required for fusion of secretory granules with the APM.

#### **RalA interacts genetically with Zonda and is required for glue granule fusion with the plasma membrane**

Given that Zda is not required for GG biogenesis or maturation, but necessary for fusion of GGs to the plasma membrane, we hypothesized that Zda may participate in docking, priming, triggering or fusion of GGs to the APM, so we performed a loss-of-function screen aimed at identifying genes that participate in these processes, which may cooperate with Zda in exocytosis of GGs. We focused particularly on genes highly expressed at the salivary gland, according to high throughput data compiled at flybase (flybase.org). We expressed in salivary glands double stranded RNAs or dominant negative alleles of candidate genes, which included Rabs<sup>25</sup>, SNAREs<sup>26</sup>, the subunits of the exocyst complex<sup>27</sup>, the small GTPase RalA<sup>28</sup>, Synaptotagmins<sup>29</sup>, AP proteins<sup>30</sup>, RE-PM contact site proteins<sup>31</sup>, and calcium channels<sup>32</sup> (Supplementary Table 1). As a read out for the

screen, we looked at SGS3-GFP retention in prepupae (Figure 4). Loss of function of 18 out of the 64 genes analyzed provoked retention of SGS3-GFP with a penetrance of 50% or higher (Supplementary Table 1 and Supplementary Figure 2).

The retention phenotype after suppressing the activity of these 18 candidate genes was further analyzed by confocal microscopy, specifically by looking at GG size and actin polymerization around the GGs. Out of the 18 candidates, loss of function of 15 of the genes resulted in blockage of GG biogenesis and/or maturation, since no GGs or very small GGs were detected (Supplementary Figure 3A, B). Among these 15 genes were the eight subunits of the exocyst complex; the small GTPase Rab1, known to mediate dynamic membrane trafficking between ER and Golgi<sup>33</sup>; the adaptor proteins Ap-1-2 $\beta$  and the Arf GEF Sec71, previously reported as essential for GG biogenesis<sup>5,34</sup>; and the syntaxins Syx5 and Syx7, Sec20, and Syt4 (Supplementary Figure 3E and Supplementary Figure 6). On the other hand, two of the hits, Rab11 and EpsinR, resulted in mature GGs that appeared covered with filamentous actin, although mislocalized at the basolateral domain of the cell (Supplementary Figure 3C, E). Finally, one remarkable hit was the small GTPase RalA, whose loss of function resulted in GGs of mature size (Figure 6A-C; Supplementary Figure 3D, E) that never fuse with the plasma membrane, do not contain PI(4,5)P<sub>2</sub>, and are not surrounded by polymerized actin (Figure 6D-G).

Given the similarities between Zda and RalA knock down phenotypes, we analyzed possible genetic interactions between the two genes. Over-expression of Zda led to partial although consistent rescue of the RalA knock-down phenotype (Figure 6H), suggesting that Zda and RalA may cooperate on the fusion of GGs to the plasma membrane. Next, we took advantage of Zda capacity to rescue the RalA loss-of-function phenotype to test the requirement of different Zda domains in GG exocytosis. We found that the Zda transmembrane domain, but not the Cam/TPR domains, is required for this Zda function (Figure 6H).

RalA was previously described to operate as an effector of the exocyst complex during tethering of secretory vesicles to the plasma membrane<sup>35,36</sup>. Loss of function of subunits of the exocyst results in immature small GGs (Supplementary Figure 6), suggesting that the exocyst complex is required for their maturation in a RalA-independent manner. These observations do not rule out an additional role of the exocyst at a later step of exocytosis for tethering GG to the plasma membrane, perhaps in cooperation with RalA and Zda.

Overall, we have identified Zda as an important player in the process of regulated exocytosis, executing its action at the final steps of the process, just prior to fusion of secretory granules with the APM, likely cooperating with the small GTPase RalA (Figure 7).

## DISCUSSION

In this work we have shown that the *Drosophila* transmembrane immunophilin Zda is highly expressed in secretory tissues, and critically required for regulated exocytosis. In the PG Zda regulates exocytosis of the molting hormone 20E; in IPCs is required for Dilp2 exocytosis, and in salivary glands it controls exocytosis of mucin-containing glue granules. Unlike other genes previously reported to contribute to *Drosophila* salivary gland secretion, such as AP-1<sup>5</sup>, PI4K<sup>37</sup>, Arl1 and Sec71<sup>34</sup>, Hobbit<sup>38</sup> and Tango1<sup>4</sup>, Zda is not required for GG biogenesis, but rather at the final steps of the exocytic process.

FKBPs are believed to operate as molecular platforms assisting the interaction of components of multi-molecular complexes<sup>12-16</sup>. FKBP8, Zda's most closely related mammalian ortholog, has been assigned multiple cellular functions that range from co-chaperone activity in the folding and trafficking of HERG channel<sup>39</sup>, anti-apoptotic activity by controlling localization of Bcl-2 and Bcl-XL at the mitochondria<sup>40</sup>, and control of cell growth, by indirect regulation of TOR activity<sup>41</sup>. More recently, we have defined a role of FKBP8 in mitophagy, acting as a mitochondrial receptor

through its interaction with LC3<sup>11</sup>. The final steps of exocytosis, from secretory granule docking to secretory granule fusion with the plasma membrane, require the concatenated action of dozens of proteins<sup>42</sup>. Thus, it is conceivable that a molecular platform on which these actions are sequentially organized is required, and Zda could provide such molecular platform. Our data in the current study suggest that the Zda transmembrane domain, but not the CaM/TRP domains, is required for exocytosis. Given that the latter domains are essential for *Drosophila* viability; it seems reasonable that they are required in other cellular processes. Thus, Zda probably fulfills diverse cellular functions as it is the case of mammalian FKBP8.

It was previously shown that Rho1 is recruited to GGs, presumably from the apical plasma membrane, after the GGs fuse with the APM to induce formation of the acto-myosin coat around GGs<sup>7</sup>. Based on the analysis of fusion markers, we conclude that Zda is required for GG fusion with the APM, and thus, Zda probably operates upstream of Rho1. This conclusion is also supported by our observations in the ring gland, where Zda depletion prevents exocytic vesicles from fusing with the plasma membrane, as indicated by accumulation of Syt-1 positive vesicles intracellularly, which results in low levels of this protein at the plasma membrane.

Our genetic screen has identified RalA as the only gene, out of 64 candidates analyzed, whose knock down phenotype resembles that of Zda loss of function. RalA is a small GTPase of the Ras superfamily believed to participate in tethering exocytic vesicles to the plasma membrane through its interaction with the exocyst complex<sup>35,43-45</sup>. Given the previously described function of RalA as a mediator of docking or anchoring of exocytic vesicles to the plasma membrane<sup>44,45</sup>, together with the similarities of the loss of function phenotypes of RalA and Zda and the genetic interaction data between the two genes, we postulate that Zda might be required at some point in between docking and membrane fusion of the SG to the plasma membrane.

Overall, we have defined the immunophilin Zda as a novel player in the process of regulated exocytosis in different organs throughout development. Zda does not play a role in GG biogenesis, and we have narrowed down its window of action to the steps that precede GG-APM fusion. Even though further research is required to define its precise molecular function, we propose that Zda might operate as a molecular platform where different molecules involved in the fusion process interact with each other.

## EXPERIMENTAL PROCEDURES

### Fly stocks and genetics

All fly stocks and crosses were kept on standard corn meal/agar medium at 25 °C, except for the crosses involving RNAi that were kept at 29°C. Crosses were set up in vials containing 5 males and five females of the required genotypes. Crosses were flipped every 24 hours to avoid larval overcrowding. Embryo collecting cages were set up using 40-50 females and 10-20 males of the required genotypes. Agar plates were changed every 12 hours, and plates were left at 25C for another 12 hours, and 1<sup>st</sup> instar larvae of the desired genotypes were sorted to vials to allow larval development.

The following *D. melanogaster* lines were from the Bloomington *Drosophila* Stock Center (<http://flystocks.bio.indiana.edu>): *sgs3-GFP* (BL5884), *sgs3-GFP* (BL5885), *UAS-white<sup>RNAi</sup>* (BL33613), *actin-Gal4* (BL4414), *forkhead-Gal4* (BL78060), *UAS-lifect-ruby* (BL35545), *UAS-dicer2* (BL24650), *UAS-PLC $\gamma$ -PH-EGFP* (BL58362), *Zda<sup>trojan</sup>* (BL77787), *dilp2-Gal4* (BL37516). *UAS-zda<sup>RNAi</sup>* (v106020) was obtained from the Vienna *Drosophila* RNAi Center (<https://stockcenter.vdrc.at>). *zda<sup>null</sup>* and *UAS-mCh-Zda* were previously reported <sup>18</sup>; *sgs3-dsRed* was generated by A. Andres' Lab <sup>6</sup>; *P0206-Gal4* and *phantom-Gal4* were gifts from P. Leopold. UAS-RNAi lines used in the screen (Supplementary Table 1) were obtained from the Bloomington *Drosophila* Stock Center

(<http://flystocks.bio.indiana.edu>) or from the Vienna Drosophila Stock Center (<https://stockcenter.vdrc.at>).

### **Cloning and transgenic line generation**

cDNA encoding full length *Zda* or its truncated versions (deletion of aminoacids 190-320 =  $Zda^{\Delta CaM/\Delta TPR}$ ; deletion of aminoacids 375-395 =  $Zda^{\Delta TM}$ ) were cloned into ENTR-mCherry vector using Eco-RI site on N-terminal and Not-I on C- terminal; then gateway into the pUAST plasmids. The plasmids pUAST-mCherry-*Zda*- $\Delta CaM/\Delta TM$  were used to generate transgenic flies. Transformants were produced by BestGene inc. (Chino Hills, CA, USA) using methodology based on procedures described previously <sup>46</sup>.

### **Tissue staining, visualization and image processing**

Tissues were dissected in PBS (137 mM NaCl, 2.7 mM KCl, 4.3 mM Na<sub>2</sub>HPO<sub>4</sub>, 1.47 mM KH<sub>2</sub>PO<sub>4</sub>, [pH 8]) and either fixed in 4% methanol-free formaldehyde for 30 minutes at room temperature, or imaged directly under confocal microscope. For filamentous actin staining, fixed tissues were incubated for 2 hours with Alexa Fluor 546 Phalloidin (ThermoFisher Scientific 1:400) in PBS-0.1% Triton X-100 (PT). When needed, 300 nM 4',6-diamidino-2-phenylindole (DAPI) was simultaneously added. For antibody staining, fixed tissues were washed three times in PT and blocked with PT bovine serum albumin 5%. Primary antibodies were incubated overnight at 4°C followed by 3 washes with PT, and 4-hour incubation with fluorophore-conjugated secondary antibodies. Primary antibodies used in this study were guinea pig anti-PTTH (1:400)<sup>47</sup>, rat anti-Dilp2 (1:400)<sup>48</sup>, gift from Leopold's Lab, and anti-GFP (1:10.000, chicken, Sigma G6539). Secondary antibodies used were Alexa Fluor 488 anti-chicken (1:400, Thermo Fisher Scientific), Alexa Fluor 546

anti-rat (1:400), Alexa Fluor 648 anti-guinea pig (1:400). Stained tissues were mounted in gelvatol mounting medium (Sigma) and imaged.

Images were captured using a Carl Zeiss confocal microscope LSM 710 with a Plan-Apochromat 63X/1.4NA oil objective, or a Carl Zeiss LSM 880 with a Plan-Apochromat 20X/0.8NA, or a Leica SP5 DS 40X objective. Insets of Figure 2E, were captured using Airyscan superresolution and Z-stacks were imaged in 100nm steps, pixel resolution of 1532x1532, and reconstructed using Zen-Zeiss software. Glue granules three-dimensional reconstructions were performed with Imaris software from Bitplane (Oxford Instruments), using confocal Z-stacks comprising up to 35 optical slices with a step size of 200nm. Images were processed using ImageJ (NIH, Bethesda, MD) according to adjust contrast and/or merge files.

### **Developmental Timing Curves**

Developmental timing experiments were done at 25°C. Three to four-hour time cuts of embryos laid on apple juice plus yeast paste plates were aged for 20 hours at which point freshly ecdysing L1 larvae were transferred to vials. Each vial contained 45 L1s as indicated in each experiment. The time until pupariation was scored every 6 hours; data from at least 3 vials were compiled.

### **Rescue by 20-hydroxyecdysone feeding**

Four-hour egg collections were made on agar plates, and after 20 hours L1 larvae were collected and grown at a density of 40 animals per vial at 18°C. At 3<sup>rd</sup> larval instar, larvae were transferred to fresh vials, and maintained 25°C until pupariation. The latter vial was supplemented or not with 20-hydroxyecdysone every 12 h (Cayman Chemical, dissolved in 95% ethanol, final



concentration of 0.2 mg/mL) until puparium formation. The time of pupariation was scored as above (Developmental Timing Curves).

### **Raising L2 Larvae for Timed Sample Collections for Ecdysone titers**

Timed samples were raised at 25°C. Forty newly-ecdysed L1s, precisely timed on apple juice collection plates, were transferred at 1-hour intervals to 35 mm plates containing agar with surface granules of live baker's yeast, and let them develop for ~20 hours. At this time point, larvae were monitored for morphological features of second instar to assess ecdysis. Two hour collections of freshly ecdysed L2s were transferred to fresh plates and let them develop until L2-L3 ecdysis, ~24 h for *phm>dcr2* and ~36 h for *phm>zda-RNAi dcr2*. Staged larvae were removed from the medium, washed twice in water, dried on a Kimwipe, and stored at -80.

### **Ecdysone Titters**

Biological replicates of 40-60 larvae were homogenized twice in methanol and cleared by centrifugation and brought to a final volume of 450 µl. Duplicate samples were dried and resuspended in 50 µl EIA buffer (spi bio 20-HE ELISA kit – A05120), and measured with a Spi Bio Kit for 20-HE ELISA following manufacturer's recommendations. The standard curve was built using GraphPad Prism software, non-linear regression curve fit.

### **Pupal size determination**

For pupal volume estimation 20-30 1<sup>st</sup> instar larvae of the desired genotype were transferred to food vials with 4% corn meal and grown at 29°C, and pupae were photographed under dissection microscope. Pupal length (L) and diameter (D) were measured using ImageJ, and pupal volume was calculated as previously reported<sup>49</sup>.

### **Dilp2 quantification**

For Dilp2 quantification in IPCs, larvae were sorted 24h after egg lay, and 40 individuals of the desired genotype transferred to vials with 4% corn meal and grown at 29°C. Early 3<sup>rd</sup> instar larvae before reaching the critical weight, were transferred to agar plates for 14-16h (starvation treatment), brains were dissected in PBS, and fixed in methanol free formaldehyde 4% for 30 minutes at room temperature, then washed 3 times for 15 min with 0,3% Triton X-100 in PBS, and blocked in 5% BSA, 0,3% Triton X-100 in PBS for 2hs. Samples were then incubated with rat anti-dilp2 (1:500) (kind gift of Pierre Leopold) overnight at 4°C, and then with an Alexa 647 anti-rat secondary antibody (Sigma 1:250). Stained samples were mounted in gelvatol mounting medium (Sigma) and imaged under a Carl Zeiss LSM 880 confocal microscope with a Plan-Apochromat 20X/0.8NA objective, with 8-bit color depth, 2,5x digital zoom and pixel resolution of 1024 x 1024. Z-stacks were imaged in 2,97µm steps over a total depth of 32,16 µm. Fluorescence quantification was assessed using ImageJ. Fluorescence intensities from all the slices were summed, and areas were selected based on the channel showing IPCs. Maximum Z-projections were made with Zen-Zeiss software.

### **Sgs3-GFP retention phenotype**

Larvae or prepupae of the desired genotype and developmental stage were visualized and photographed inside vials under a fluorescence dissection microscope. Each experiment was repeated at least 3 times.

### **Statistical analyses**

Statistical significance was calculated using the two-tailed Student's t test when comparing two values, and one-way analysis of variance (ANOVA) or Deviance analysis, followed by a Tuckey's test with a 95% confidence interval ( $p < 0.05$ ) when comparing multiple values. When needed, Grubb's test was used to identify the values that were significant outliers from the rest ( $p < 0.05$ ) (<https://graphpad.com/quickcalcs/grubbs2/>). In all cases, error bars represent the SD.

#### COMPETING INTERESTS

The authors declare no competing or financial interests.

#### FUNDING

This work was supported by Agencia Nacional de Promoción Científica y Tecnológica (ANPCyT) grants PICT 2011-0090, PICT 2012-0214, PICT 2015-0649 and PICT 2017-1356 to P.W. and PICT 2011-2556 and PICT 2012-2376 to M.M.; R.V.R.-C. and S.P. are doctoral fellows of Consejo Nacional de Investigaciones Científicas y Técnicas (CONICET) and ANPCyT; S.S. is an undergraduate fellow of Consejo Interuniversitario Nacional (CIN); P.W. and M.M. are career researchers of CONICET.

#### REFERENCES

1. Sugita S. Mechanisms of exocytosis. *Acta Physiol.* 2007;192(2):185-193. doi:10.1111/j.1748-1716.2007.01803.x
2. Biyasheva A, Do TV, Lu Y, Vaskova M, Andres AJ. Glue secretion in the Drosophila salivary gland: A model for steroid-regulated exocytosis. *Dev Biol.* 2001;231(1):234-251. doi:10.1006/dbio.2000.0126
3. Tran DT, Ten Hagen KG. Real-time insights into regulated exocytosis. *J Cell Sci.* 2017;130(8):1355-1363. doi:10.1242/jcs.193425
4. Reynolds HM, Zhang L, Tran DT, Ten Hagen KG. Tango1 coordinates the formation of endoplasmic reticulum/ Golgi docking sites to mediate secretory granule formation. *J Biol Chem.* 2019;294(51):19498-19510. doi:10.1074/jbc.RA119.011063
5. Burgess J, Jauregui M, Tan J, et al. AP-1 and clathrin are essential for secretory granule biogenesis in Drosophila. *Mol Biol Cell.* 2011;22(12):2094-2105. doi:10.1091/mbc.E11-01-0054
6. Costantino BFB, Bricker DK, Alexandre K, et al. A Novel Ecdysone Receptor Mediates Steroid-Regulated Developmental Events during the Mid-Third Instar of Drosophila. Rulifson E, ed. *PLoS Genet.* 2008;4(6):e1000102. doi:10.1371/journal.pgen.1000102
7. Rousso T, Schejter ED, Shilo BZ. Orchestrated content release from Drosophila glue-protein vesicles by a contractile actomyosin network. *Nat Cell Biol.* 2016;18(2):181-190.

doi:10.1038/ncb3288

8. Tran DT, Masedunskas A, Weigert R, Ten Hagen KG. Arp2/3-mediated F-actin formation controls regulated exocytosis in vivo. *Nat Commun*. 2015;6:1-10. doi:10.1038/ncomms10098
9. Kang CB, Hong Y, Dhe-Paganon S, Yoon HS. FKBP Family Proteins: Immunophilins with Versatile Biological Functions. *Neurosignals*. 2008;16(4):318-325. doi:10.1159/000123041
10. Ghartey-Kwansah G, Li Z, Feng R, et al. Comparative analysis of FKBP family protein: Evaluation, structure, and function in mammals and *Drosophila melanogaster*. *BMC Dev Biol*. 2018;18(1):7. doi:10.1186/s12861-018-0167-3
11. Bhujabal Z, Birgisdottir ÁB, Sjøttem E, et al. FKBP8 recruits LC3A to mediate Parkin-independent mitophagy. *EMBO Rep*. 2017;18(6):947-961. doi:10.15252/embr.201643147
12. Haupt K, Jahreis G, Linnert M, et al. The FKBP38 catalytic domain binds to Bcl-2 via a charge-sensitive loop. *J Biol Chem*. 2012;287(23):19665-19673. doi:10.1074/jbc.M111.317214
13. Chen Y, Sternberg P, Cai J. Characterization of a Bcl-X L-interacting protein FKBP8 and its splice variant in human RPE cells. *Investig Ophthalmol Vis Sci*. 2008;49(4):1721-1727. doi:10.1167/iovs.07-1121
14. Okamoto T, Nishimura Y, Ichimura T, et al. Hepatitis C virus RNA replication is regulated by FKBP8 and Hsp90. *EMBO J*. 2006;25(20):5015-5025. doi:10.1038/sj.emboj.7601367
15. Shimamoto S, Tsuchiya M, Yamaguchi F, Kubota Y, Tokumitsu H, Kobayashi R. Ca<sup>2+</sup>/S100 proteins inhibit the interaction of FKBP38 with Bcl-2 and Hsp90. *Biochem J*. 2014;458(1):141-152. doi:10.1042/BJ20130924
16. Bai X, Ma D, Liu A, et al. Supporting Online Material Rheb Activates mTOR by Antagonizing Its Endogenous Inhibitor, FKBP38. *Proc Natl Acad Sci USA*. 2001;2:10932. doi:10.1126/science.1149121
17. Barth S, Nesper J, Hasgall PA, et al. The Peptidyl Prolyl cis/trans Isomerase FKBP38 Determines Hypoxia-Inducible Transcription Factor Prolyl-4-Hydroxylase PHD2 Protein Stability. *Mol Cell Biol*. 2007;27(10):3758-3768. doi:10.1128/mcb.01324-06
18. Melani M, Valko A, Romero NM, et al. Zonda is a novel early component of the autophagy pathway in *Drosophila*. *Mol Biol Cell*. 2017;28(22):3070-3081. doi:10.1091/mbc.E16-11-0767
19. Diao F, Ironfield H, Luan H, et al. Plug-and-play genetic access to drosophila cell types using exchangeable exon cassettes. *Cell Rep*. 2015;10(8):1410-1421. doi:10.1016/j.celrep.2015.01.059
20. Gelbart, W.M., Emmert DB. FlyBase High Throughput Expression Pattern Data. 2013.
21. Yamanaka N, Marqués G, O'Connor MB. Vesicle-Mediated Steroid Hormone Secretion in *Drosophila melanogaster*. *Cell*. 2015;163(4):907-919. doi:10.1016/j.cell.2015.10.022
22. Cao J, Ni J, Ma W, et al. Insight into insulin secretion from transcriptome and genetic analysis of insulin-producing cells of *Drosophila*. *Genetics*. 2014;197(1):175-192. doi:10.1534/genetics.113.160663
23. Géminard C, Rulifson EJ, Léopold P. Remote Control of Insulin Secretion by Fat Cells in

*Drosophila. Cell Metab.* 2009;10(3):199-207. doi:10.1016/j.cmet.2009.08.002

24. Phan TK, Williams SA, Bindra GK, Lay FT, Poon IKH, Hulett MD. Phosphoinositides: multipurpose cellular lipids with emerging roles in cell death. *Cell Death Differ.* 2019;26(5):781-793. doi:10.1038/s41418-018-0269-2
25. Pfeffer SR. Rab GTPases: Master regulators that establish the secretory and endocytic pathways. *Mol Biol Cell.* 2017;28(6):712-715. doi:10.1091/mbc.E16-10-0737
26. Zorec R. SNARE-mediated vesicle navigation, vesicle anatomy and exocytotic fusion pore. *Cell Calcium.* 2018;73:53-54. doi:10.1016/j.ceca.2018.03.004
27. Heider MR, Munson M. Exorcising the Exocyst Complex. *Traffic.* 2012;13(7):898-907. doi:10.1111/j.1600-0854.2012.01353.x
28. Shirakawa R, Horiuchi H. Ral GTPases: crucial mediators of exocytosis and tumorigenesis. *J Biochem.* 2015;157(5):285-299. doi:10.1093/jb/mvv029
29. Gustavsson N, Han W. Calcium-sensing beyond neurotransmitters: Functions of synaptotagmins in neuroendocrine and endocrine secretion. *Biosci Rep.* 2009;29(4):245-259. doi:10.1042/BSR20090031
30. Azarnia Tehran, López-Hernández, Maritzen. Endocytic Adaptor Proteins in Health and Disease: Lessons from Model Organisms and Human Mutations. *Cells.* 2019;8(11):1345. doi:10.3390/cells8111345
31. Saheki Y, De Camilli P. The Extended-Synaptotagmins. *Biochim Biophys Acta - Mol Cell Res.* 2017;1864(9):1490-1493. doi:10.1016/j.bbamcr.2017.03.013
32. Rizo J, Rosenmund C. Synaptic vesicle fusion. *Nat Struct Mol Biol.* 2008;15(7):665-674. doi:10.1038/nsmb.1450
33. Plutner H, Cox AD, Pind S, et al. Rab1b regulates vesicular transport between the endoplasmic reticulum and successive Golgi compartments. *J Cell Biol.* 1991;115(1):31-43. doi:10.1083/jcb.115.1.31
34. Torres IL, Rosa-Ferreira C, Munro S. The Arf family G protein Arl1 is required for secretory granule biogenesis in *Drosophila*. *J Cell Sci.* 2014;127(10):2151-2160. doi:10.1242/jcs.122028
35. Jin R, Junutula JR, Matern HT, Ervin KE, Scheller RH, Brunger AT. Exo84 and Sec5 are competitive regulatory Sec6/8 effectors to the RalA GTPase. *EMBO J.* 2005;24(12):2064-2074. doi:10.1038/sj.emboj.7600699
36. Moskalenko S, Henry DO, Rosse C, Mirey G, Camonis JH, White MA. The exocyst is a Ral effector complex. *Nat Cell Biol.* 2002;4(1):66-72. doi:10.1038/ncb728
37. Burgess J, Del Bel LM, Ma C-IJ, et al. Type II phosphatidylinositol 4-kinase regulates trafficking of secretory granule proteins in *Drosophila*. *Development.* 2012;139(16):3040-3050. doi:10.1242/dev.077644
38. Neuman SD, Bashirullah A. Hobbit regulates intracellular trafficking to drive insulin-dependent growth during *Drosophila* development. *Development.* 2018;145(11):dev161356. doi:10.1242/dev.161356

39. Walker VE, Atanasiu R, Lam H, Shrier A. Co-chaperone FKBP38 promotes HERG trafficking. *J Biol Chem*. 2007;282(32):23509-23516. doi:10.1074/jbc.M701006200
40. Shirane M, Nakayama KI. Inherent calcineurin inhibitor FKBP38 targets Bcl-2 to mitochondria and inhibits apoptosis. *Nat Cell Biol*. 2003;5(1):28-37. doi:10.1038/ncb894
41. Bai X, Ma D, Liu A, et al. Rheb activates mTOR by antagonizing its endogenous inhibitor, FKBP38. *Science (80- )*. 2007;318(5852):977-980. doi:10.1126/science.1147379
42. Wang H, Zhang C, Xiao H. Mechanism of membrane fusion: protein-protein interaction and beyond. *Int J Physiol Pathophysiol Pharmacol*. 2019;11(6):250-257. <http://www.ncbi.nlm.nih.gov/pubmed/31993099>. Accessed April 26, 2020.
43. Chen XW, Leto D, Chiang SH, Wang Q, Saltiel AR. Activation of RalA Is Required for Insulin-Stimulated Glut4 Trafficking to the Plasma Membrane via the Exocyst and the Motor Protein Myo1c. *Dev Cell*. 2007;13(3):391-404. doi:10.1016/j.devcel.2007.07.007
44. Teodoro RO, Pekkurnaz G, Nasser A, et al. Ral mediates activity-dependent growth of postsynaptic membranes via recruitment of the exocyst. *EMBO J*. 2013;32(14):2039-2055. doi:10.1038/emboj.2013.147
45. Holly RM, Mavor LM, Zuo Z, Blankenship JT. A rapid, membrane-dependent pathway directs furrow formation through RalA in the early *Drosophila* embryo. *Development*. 2015;142(13):2316-2328. doi:10.1242/dev.120998
46. Rubin GM, Spradling AC. Genetic transformation of *Drosophila* with transposable element vectors. *Science (80- )*. 1982;218(4570):348-353. doi:10.1126/science.6289436
47. Yamanaka N, Romero NM, Martin FA, et al. Neuroendocrine control of *Drosophila* larval light preference. *Science (80- )*. 2013;341(6150):1113-1116. doi:10.1126/science.1241210
48. Géminard C, Arquier N, Layalle S, et al. Control of metabolism and growth through insulin-like peptides in *Drosophila*. *Diabetes*. 2006;55(SUPPL. 2):S5-S8. doi:10.2337/db06-S001
49. Galagovsky D, Katz MJ, Acevedo JM, Sorianello E, Glavic A, Wappner P. The *Drosophila* insulin-degrading enzyme restricts growth by modulating the PI3K pathway in a cell-autonomous manner. *Mol Biol Cell*. 2014;25(6):916-924. doi:10.1091/mbc.E13-04-0213

## FIGURE LEGENDS

**Figure 1. Zonda is expressed in secretory tissues.** The *zda<sup>trojan</sup>* line was crossed to UAS-mCD8-GFP flies, and tissues were dissected and observed directly under the confocal microscope. Larval salivary gland (A), ring gland (B), brain (C), lymph gland (D), intestine (E), fat body (F), eye imaginal disc (G), wing imaginal disc (H), adult male accessory gland (I), ejaculatory duct (J), testis (K), adult female egg chambers (L). For comparative purposes all images were acquired using the same microscope set up.

**Figure 2. Zonda is required for ecdysone exocytosis at the prothoracic gland.** (A) *zda<sup>trojan</sup>* is expressed at high levels in the prothoracic gland (PG), as revealed by visualization of mCD8-GFP (green) that coincides with PPTH-labeled axons (red). (B) Pupuration time was recorded in control (*phantom<white<sup>RNAi</sup>*) and Zda knock-down larvae (*phantom<zda<sup>RNAi</sup>*) that were grown either in

control media or media supplemented with ecdysone (20E). (C) Quantification by ELISA of 20E levels in hemolymph relative to levels of total 20E in L2 larvae homogenates; \*  $p < 0.05$ . (D-E) Confocal images of wandering larvae ring glands that express Synaptotagmin-1-GFP (green) under control of *P0206-Gal4*. (D) Control ring glands (*UAS-white<sup>RNAi</sup>*) and (E) Zda knock-down ring glands (*UAS-zda<sup>RNAi</sup>*) are compared. Insets: (D') Synaptotagmin is mostly concentrated at the plasma membrane in control individuals (white arrows), while the number of intracellular vesicles labeled with syt-1-GFP is low (yellow arrows); (E') in Zda knock-down larvae many syt-1-GFP vesicles can be observed inside PG cells (yellow arrows); the insets below show magnified images of the vesicles boxed in panel E'. Scale bars: D, E = 20 $\mu$ m, D', E' = 2 $\mu$ m. (F) quantification of Syt-1 positive vesicles detected in each genotype. N = 3 for each genotype. \*\*\* $p < 0.001$ .

**Figure 3. Zonda is required in Insulin Producing Cells for Dilp2 exocytosis.** (A) *Zda<sup>trojan</sup>* expression is high in IPCs, as revealed by mCD8-GFP expression (green), and colocalization with Dilp2 (red). (B) Downregulation of *Zda* in IPCs (*dilp2 < zda<sup>RNAi</sup>*) provokes reduction of pupal volume compared to control pupae (*dilp2 < white<sup>RNAi</sup>*). Representative images are shown. Control: N = 85; *zda<sup>RNAi</sup>*: N = 65. (C, D) Zda downregulation provokes accumulation of Dilp2 in IPCs even under feeding conditions; the Dilp2 signal in IPCs of 3<sup>rd</sup> instar larvae upon 16 hours starvation was compared to that of fed individuals. (C) Dilp2 was detected by immunofluorescence (green), while IPCs were identified by expression of UAS-cherry under the control of Dilp2-Gal4 (red). Representative images are shown. (D) Quantification of the average fluorescence intensity in the experiment of panel (C). *white<sup>RNAi</sup>* fed N = 24; *white<sup>RNAi</sup>* starved N = 24; *zda<sup>RNAi</sup>* fed N = 19; *zda<sup>RNAi</sup>* starved N = 30. \*\*  $p < 0.01$ ; \*\*\*  $p < 0.001$ . Scale bar = 50  $\mu$ m.

**Figure 4. Zonda is required in salivary glands for Glue granule exocytosis.** (A-D) Secretion of Sgs3-GFP (green) in control and Zda-knock down larvae and prepupae. Larvae of both genotypes accumulate comparable levels of Sgs3-GFP in their salivary glands (A, A' and C, C'). After pupation, control larvae have secreted Sgs3-GFP, which is extruded outside the puparium (B, B'), while *zda<sup>RNAi</sup>* prepupae retain Sgs3-GFP inside their salivary glands (D, D'). (E) quantification of Sgs3-GFP retention inside salivary glands in prepupae; N = 192 for *white<sup>RNAi</sup>* and N = 133 for *zda<sup>RNAi</sup>*. \*\*  $p < 0.01$ . (F, G) Sgs3-GFP is retained inside salivary gland cells in Zda-knock down prepupae. Confocal images of control (*white<sup>RNAi</sup>*) and Zda-knock down (*zda<sup>RNAi</sup>*) prepupal salivary glands; Sgs3-GFP-labeled Glue granules (green), nuclei stained with DAPI (blue), and phalloidin (red). "L" indicates the lumen. Scale bar: 50 $\mu$ m

**Figure 5. Zonda is required for Glue granule (GG) fusion with the plasma membrane.** (A-C) Zda is not required for GG biogenesis or maturation. (A, B) Confocal images of salivary glands dissected from wandering larvae of control (*white<sup>RNAi</sup>*) (A, A') and *zda<sup>RNAi</sup>* (B, B') individuals prior to pupation expressing Sgs3-GFP (green), and labelled with phalloidin (red). "L" indicates the lumen that is also marked with a dashed line. Scale bar: 20 $\mu$ m. Crop size 20 $\mu$ m $\times$ 20 $\mu$ m. (C) Quantification of GG diameter in both genotypes; no statistical difference was detected; 40 GGs were scored for each genotype (N = 4). (D-G) Zda is required for GG fusion with the PM. (D-E) Confocal images of wandering larvae salivary glands expressing PLC $\delta$ PH-EGFP (green) and stained with phalloidin (red). While in control larvae GGs are positive for PLC $\delta$ PH-EGFP (D, D'), and stain positive for phalloidin (D, D''), *zda<sup>RNAi</sup>* GGs are negative for both markers (E-E''). Arrows mark GGs positive for PLC $\delta$ PH-EGFP and phalloidin. "L" indicates the lumen that is also marked with a dashed line. Scale bar: 20 $\mu$ m. Crop size: 15 $\mu$ m $\times$ 15 $\mu$ m. (F, G) Quantification of GGs containing PLC $\delta$ PH-EGFP (F) or phalloidin (G) in

100  $\mu\text{m}$  of plasma membrane. N= 40 for each genotype. Statistically significant differences were found for the two markers analyzed (\*  $p < 0.05$ ). (H-I) Confocal images of wandering larvae salivary glands expressing Sgs3-GFP (green), stained with phalloidin (red). In control larvae GGs are surrounded by an actin mesh, and a phalloidin-positive fusion neck that connects the GG with the APM can be seen (H). In *zda<sup>RNAi</sup>* salivary glands, neither fusion necks nor actin meshes can be detected (I). Z-stacks were acquired with a step size of 200nm and the numbers indicate the position of each optical section relative to the first section of the Z-stack. Representative images are shown. Scale bar: 5 $\mu\text{m}$ .

**Figure 6. RalA is required for Glue granule fusion with the plasma membrane.** (A-C) RalA is not required for GG biogenesis or maturation. (A-B) Confocal images of salivary glands dissected from wandering larvae of control (*white<sup>RNAi</sup>*) (A) and *ralA<sup>RNAi</sup>* (B) genotypes expressing Sgs3-GFP (green), and stained with phalloidin (red). "L" indicates the lumen that is also marked with a dashed line. Scale bar: 20 $\mu\text{m}$ . Crop size 20 $\mu\text{m}$ x20 $\mu\text{m}$ . (C) Quantification of GG diameter in both genotypes; no statistical difference was detected; 40 GGs were scored per genotype (N = 4). (D-G) RalA is required for GG fusion with the PM. (D-E) Confocal images of wandering larvae salivary glands expressing PLC $\delta$ PH-EGFP (green) and stained with phalloidin (red). While in control larvae GGs are positive for PLC $\delta$ PH-EGFP (D, D') and phalloidin (D, D''), in *ralA<sup>RNAi</sup>* individuals GGs are negative for both markers (E-E''). Arrows in D-D'' point at GGs positive for PLC $\delta$ PH-EGFP and phalloidin. "L" indicates the lumen that is also marked with a dashed line. Scale bar: 20 $\mu\text{m}$ . Crops size: 15 $\mu\text{m}$ x15 $\mu\text{m}$ . Quantification of GGs containing PLC $\delta$ PH-EGFP (F) or phalloidin (G) in 100  $\mu\text{m}$  of plasma membrane; N= 40 for each genotype. Statistically significant differences were found for the two markers analyzed (\*  $p < 0.05$ ). (H) Genetic interaction between RalA and Zda: The RalA loss-of-function retention phenotype of Sgs3-GFP in salivary glands was scored in prepupae of two different genotypes: mCh-NLS, *RalA<sup>RNAi</sup>* (N = 53) and lifeact-ruby, *RalA<sup>RNAi</sup>* (N = 51), as well as in the indicated combinations with full length or deleted versions of mCh-Zda. mCh-Zda, *white<sup>RNAi</sup>* (N = 68), mCh-Zda, *RalA<sup>RNAi</sup>* (N = 35), mCh-Zda $\Delta^{\text{Cam/TRP}}$ , *white<sup>RNAi</sup>* (N = 62), mCh-Zmda $\Delta^{\text{Cam/TRP}}$ , *RalA<sup>RNAi</sup>* (N = 62) mCh-Zda $\Delta^{\text{TM}}$ , *white<sup>RNAi</sup>* (N = 35), mCh-Zda $\Delta^{\text{TM}}$ , *RalA<sup>RNAi</sup>* (N = 13). The RalA loss-of-function phenotype was largely suppressed by overexpression of full-length mCh-Zda or mCh-Zda $\Delta^{\text{Cam/TRP}}$ , but not by overexpression of mCh-Zda $\Delta^{\text{TM}}$ . A Deviance analysis followed by Tukey test was performed.

**Figure 7. Proposed model of Zonda action in Glue granule exocytosis.** Zda operates at final stages of GG exocytosis downstream of RalA, and before GG-APM fusion.  $\text{Ca}^{++}$ /CaM-bound Zda might act as a platform for fusogenic factors, such as SNAREs and Synaptotagmin. Rho-1-induced acto-myosin recruitment to GGs occurs down-stream of Zda action.

**Supplementary Figure 1.** (A) The *zda* locus (CG5482) encompasses 5 exons. Imprecise excision of a P element (EY08359) inserted in the 5'UTR of the gene was induced, and generated a 1100 base pairs deletion giving rise to the *zda<sup>null</sup>* allele. The *Mi{Trojan-Gal4.0}zda[Mi07788-TG4.0]* insertion at the 2<sup>nd</sup> intron generates a truncated version of Zda. (B) Schematic representation of Zda predicted domains. From the N- to the C-terminus: Peptidyl prolyl cis/trans isomerase (PPIase), Calmodulin binding (CaM), Tetratricopeptide repeat (TPR), and Transmembrane (TM) domains are depicted. Deletion of specific domains used to generate transgenic lines are shown below. (C) Complementation test. Analysis of viability to adulthood of different combinations *zda* alleles.



**Supplementary Figure 2.** Quantification of Sgs3-GFP retention inside salivary glands of prepupae after loss of function of the indicated genes. RNAi or dominant negative constructs were expressed in salivary glands using a *fkh-Gal4* driver. The penetrance of the phenotypes is depicted. The number of individuals scored in each case is shown in Supplementary Table 1.

**Supplementary Figure 3.** Phenotypic categories identified at the secondary screen: A) wild type; B) Small GGs; C) delocalized GGs (DGG); D) Mature GGs without actin mesh (MGGnA). GGs are labeled with Sgs3-GFP (green), and filamentous actin is labelled with phalloidin (red); “L” indicates the lumen that is also marked with a dashed line. Scale bar: 20µm. Crop size 20µmx20µm. (E) The genes identified in each category are listed.

**Supplementary Figure 4.** Z-stack confocal images of glue granules in wandering larvae salivary glands expressing Sgs3-GFP (green), and stained with phalloidin (red). Upper: a GG of a control (*white<sup>RNAi</sup>*) larvae can be seen surrounded by an actin mesh, and connected to the APM by a fusion neck. Lower: GGs of *zda<sup>RNAi</sup>* larvae are not surrounded by an actin mesh and are not connected with the APM through fusion necks. Images were acquired with a step size of 200nm, and the numbers indicate the position of each optical section relative to the first section in the Z-stack. Representative images are shown. Scale bar: 5µm.

**Supplementary Figure 5.** Confocal images of salivary gland cells of control (A, B) or Zda deficient (C) larvae dissected at either early L3 (A) or late wandering L3 (B, C). Salivary glands express Sgs3-GFP (green) and were stained with phalloidin (red). Note that in wild type individuals, GGs that have not yet fused with the plasma membrane have an Sgs3-GFP content with a characteristic bright and heterogeneous appearance (\*), whereas GGs that have fused with the plasma membrane have a homogenous fainter content (\*\*). The number of unfused (\*) and fused GGs (\*\*) per 100µm of apical plasma membrane length at confocal sections of were scored (D). ten salivary glands were analyzed for each genotype and statistically significant differences were found for the two genotypes analyzed (N= 10). T-test, p = 0.0013.

**Supplementary Figure 6.** Glue granule phenotypes following expression of RNAi against exocyst subunits. Confocal images of salivary gland cells dissected from wandering larvae expressing a control RNAi (*white<sup>RNAi</sup>*) (A), or RNAi against the indicated subunits of the exocyst (B-H). (I) Quantification of GG diameter in each of the genotypes. Granules in cells expressing RNAi against subunits of the exocyst are significantly smaller than those of control larvae. ANOVA test followed by Tukey test was performed.

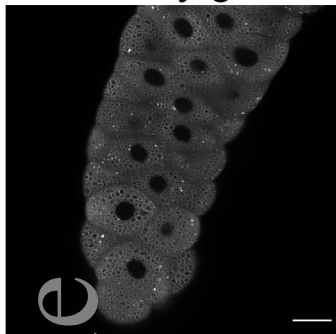
**Supplementary Video 1.** Glue granules of wild type larvae fuse with the APM, and a connecting fusion neck is visible. A GG labelled with Sgs3-GFP and surrounded by an actin mesh (phalloidin-positive). Three dimensional reconstitution of 35 confocal slices (step size: 200nm). The animation was generated with the Imaris software.

**Supplementary Video 2.** Glue granules in larvae expressing Zda RNAi fail to fuse with the APM. GGs, labelled with Sgs3-GFP do not appear surrounded by an actin mesh (phalloidin-negative), and are not connected with the APM the three dimensional reconstitution of 35 confocal slices (step size: 200nm). The animation was generated with the Imaris software.

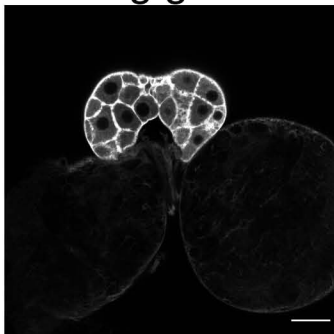
**Supplementary Table 1.** List of genes screened for Sgs3-GFP exocytosis.

*zonda*<sup>trojan</sup> < mCD8-GFP

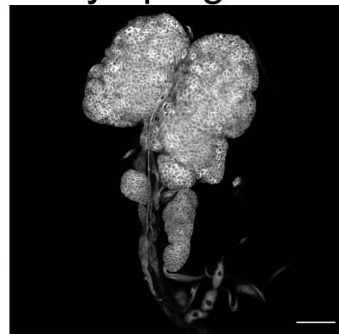
A salivary gland



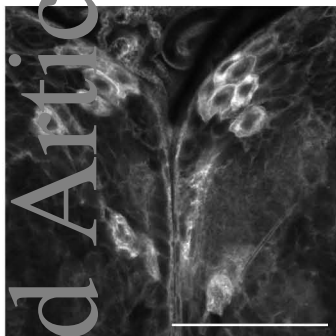
B ring gland



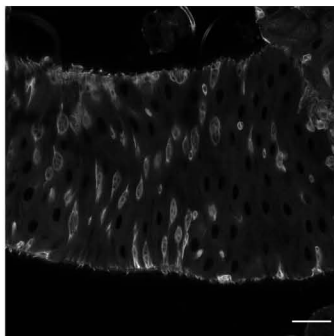
C lymph gland



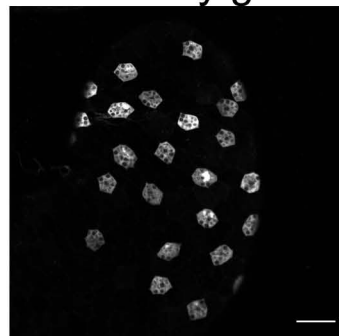
D IPCs



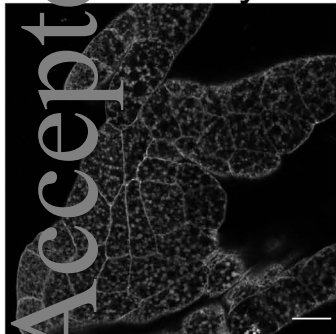
E intestine



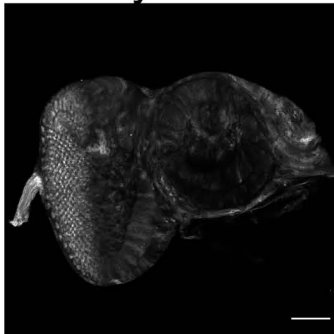
F accessory gland



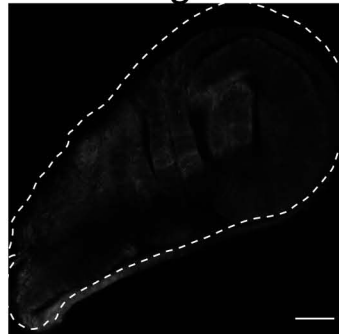
G fat body



H eye ID



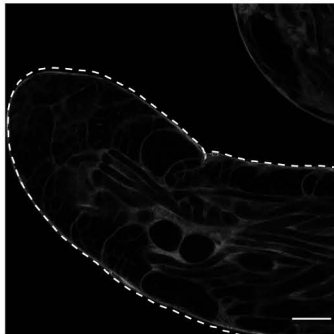
I wing ID



J eyaculatory duct



K testis

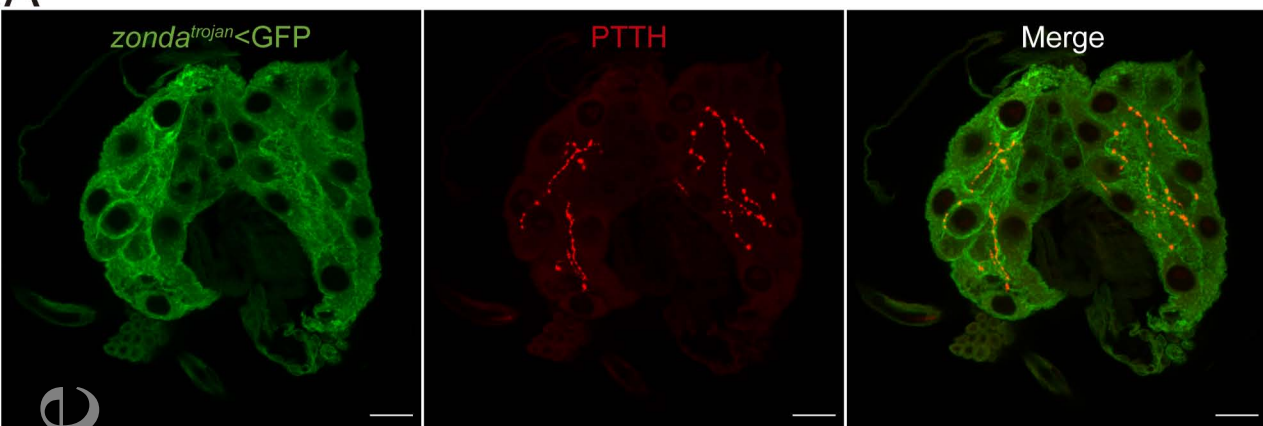


L egg chambers

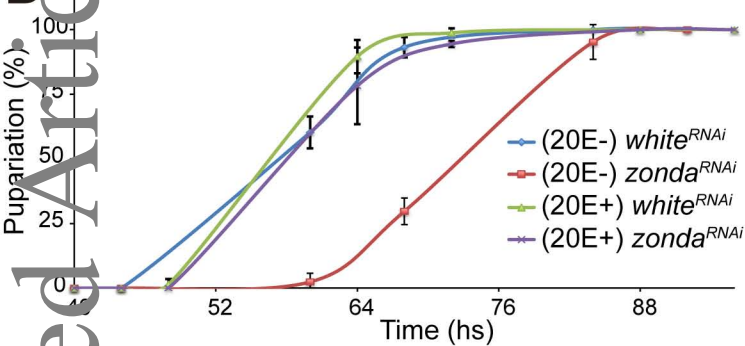


FIGURE 1

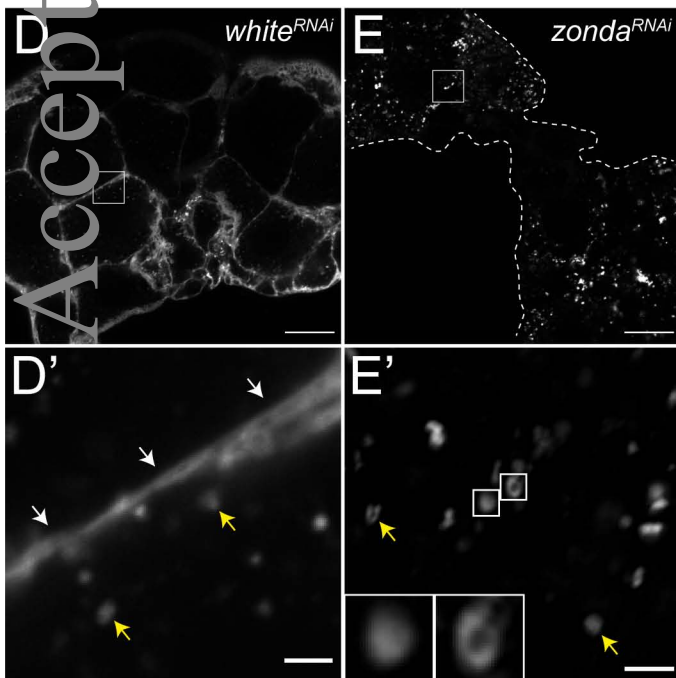
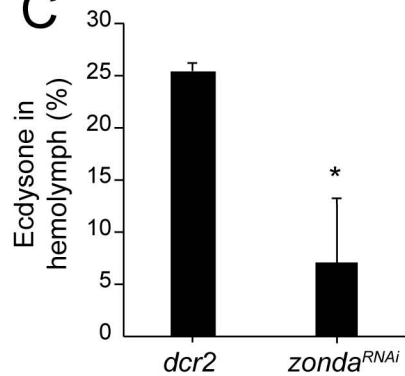
A



B



C



F

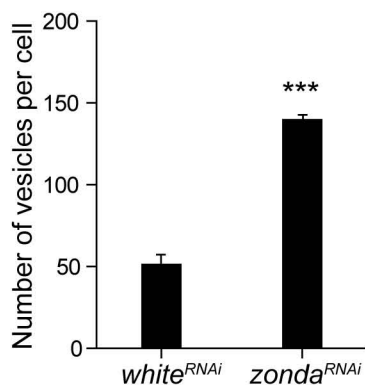


FIGURE 2

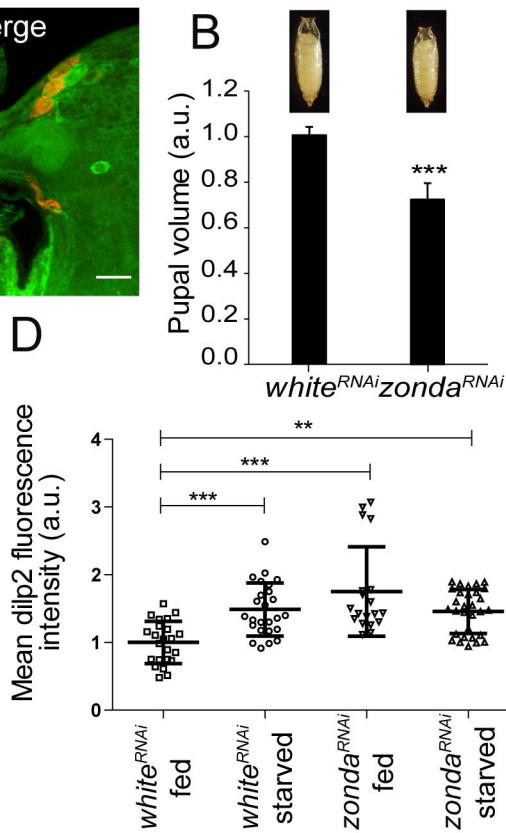
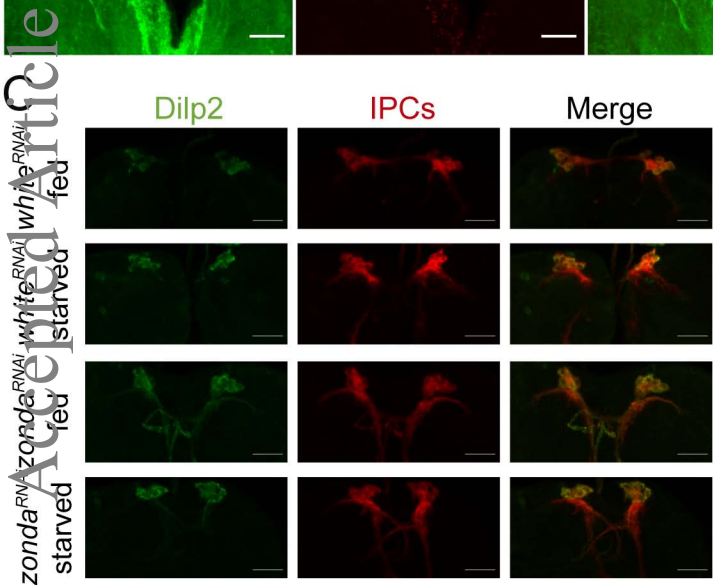
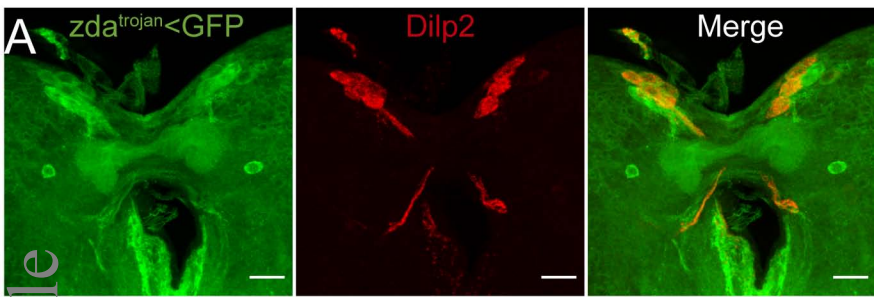


FIGURE 3

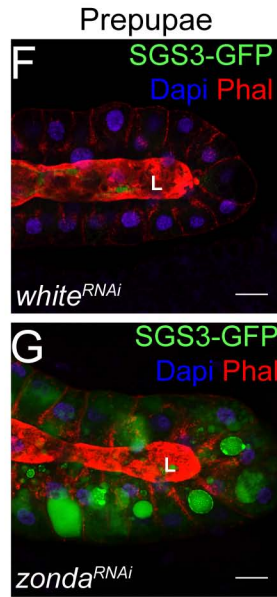
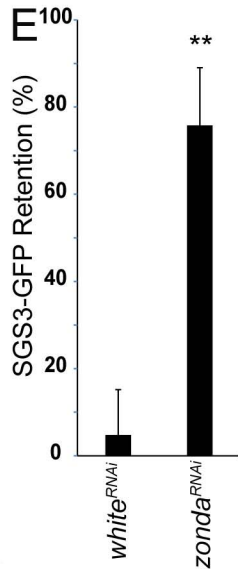
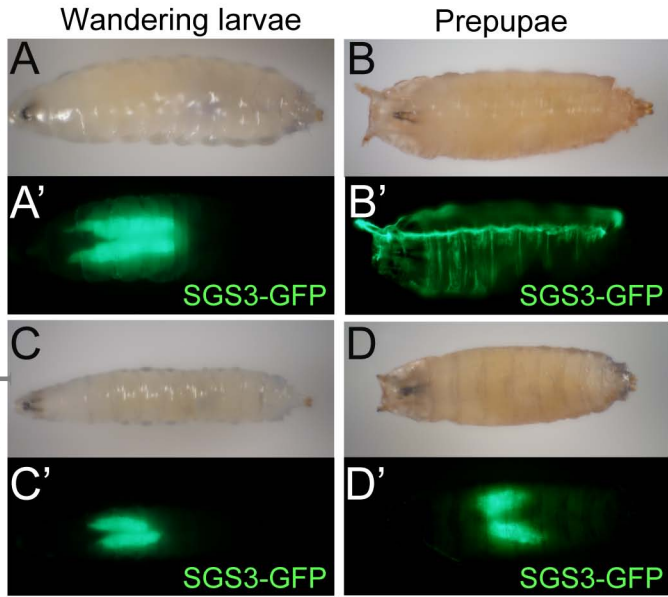


FIGURE 4

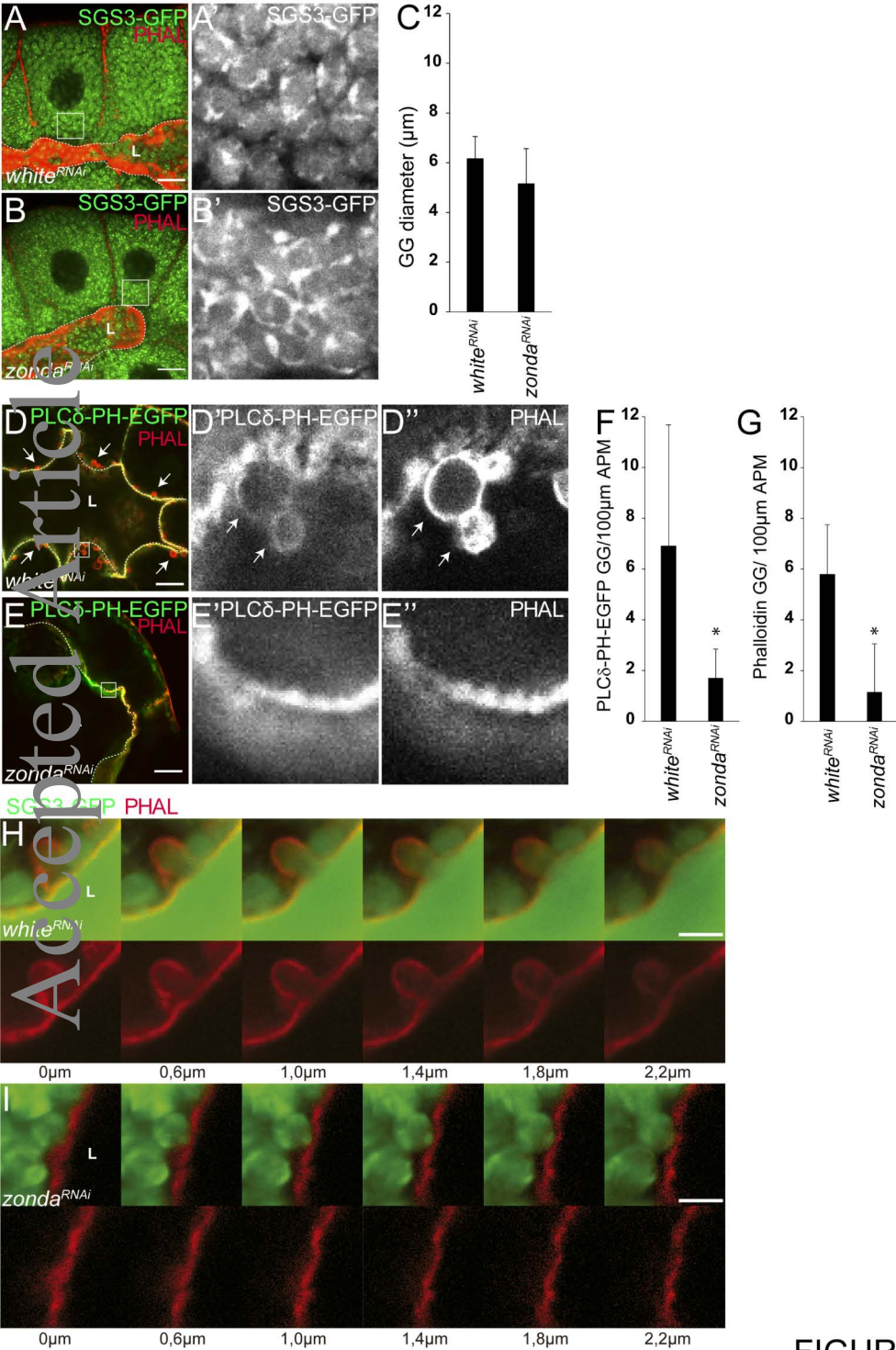
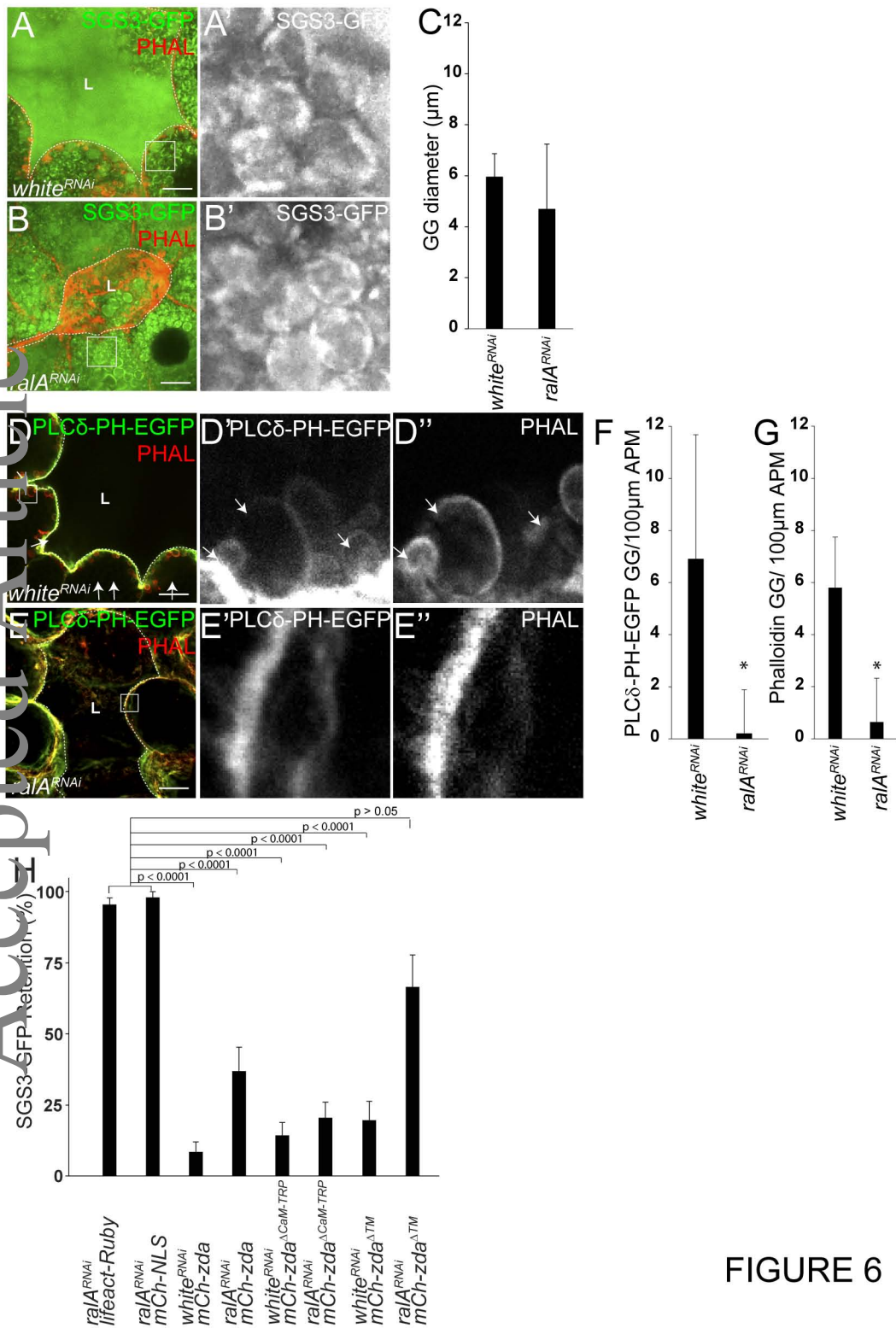


FIGURE 5





APM

Lumen

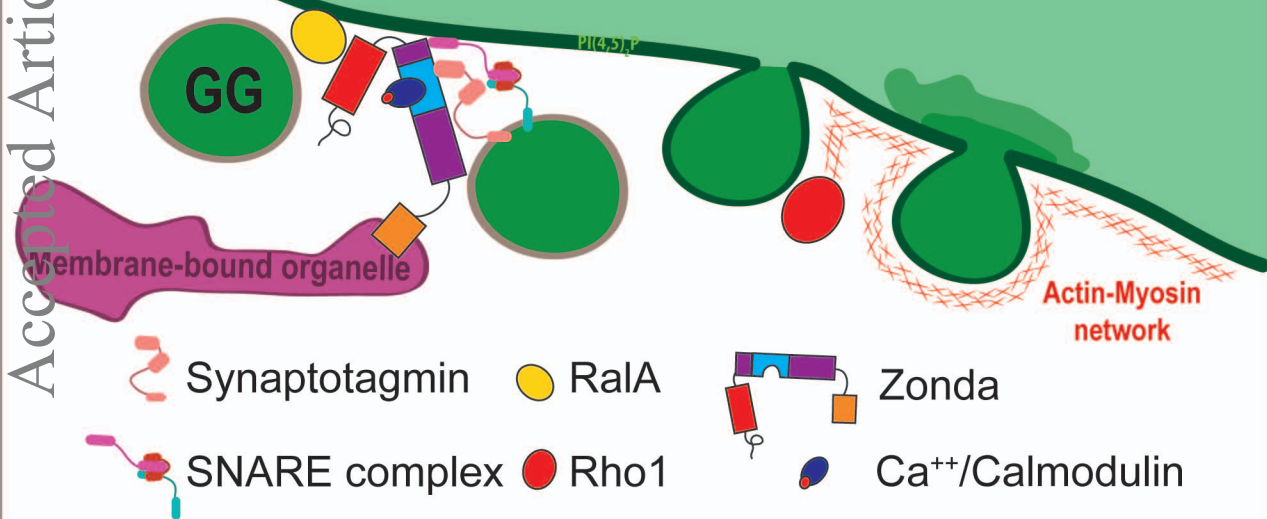


FIGURE 7